


Quantum algorithms for Schrieffer-Wolff transformation

Zongkang Zhang , Yongdan Yang , Xiaosi Xu *, and Ying Li †
 Graduate School of China Academy of Engineering Physics, Beijing 100193, China

 (Received 14 February 2022; accepted 6 September 2022; published 12 October 2022)

The Schrieffer-Wolff transformation aims to solve degenerate perturbation problems and give an effective Hamiltonian that describes the low-energy dynamics of the exact Hamiltonian in the low-energy subspace of an unperturbed Hamiltonian. This unitary transformation decoupling the low-energy and high-energy subspaces for the transformed Hamiltonian can be realized by quantum circuits. We give a fully quantum algorithm for realizing the SW transformation. We also propose a hybrid quantum-classical algorithm for finding the effective Hamiltonian on NISQ hardware, where a general cost function is used to indicate the decoupling degree. Numerical simulations without or with noise and experiments on quantum computer *ibmq_manila* are implemented for a Heisenberg chain model. Our results verify the algorithm and show its validity on near-term quantum computers.

DOI: [10.1103/PhysRevResearch.4.043023](https://doi.org/10.1103/PhysRevResearch.4.043023)

I. INTRODUCTION

Understanding and controlling quantum many-body systems is of crucial importance in modern physics [1–3]. With the exponential growth of Hilbert space, it is difficult to perform accurate analytical calculations as the system size increases. In most applications, a description of the low-energy properties is sufficient, thus the study of the low-energy effective Hamiltonian (H_{eff}) plays an important role in many-body physics [4]. The Schrieffer-Wolff transformation (SWT) was originally proposed in Ref. [5], where the Kondo model is obtained from the Anderson impurity model in the strong coupling regime with a unitary transformation. SWT extracts H_{eff} from the exact Hamiltonian by decoupling the low-energy and high-energy subspaces. It is regarded as the operator version of the degenerate perturbation theory [6]. For instance, with SWT one can infer that the half-filled Fermi-Hubbard model is equivalent to the Heisenberg model in the strong coupling limit [7,8], where the perturbation theory approach becomes impractical [9]. Being widely applied and developed in many kinds of quantum problems [10–24], SWT also has different names across various fields: the Foldy-Wouthuysen transformation in relativistic quantum mechanics [25], Fröhlich transformation in electron-phonon interaction [26], and $k \cdot p$ method in semiconductor physics [27].

SWT provides a systematic perturbative method for computing H_{eff} at any order [6]. The transformation is performed by a unitary operator defined as $U = e^S$, where S is an anti-Hermitian operator and is called the generator. The coefficients in the Taylor series of S can be derived order by order

through an inductive formula, which is hard for high orders. What's more, the calculation is carried out in the space of the whole system, which scales up exponentially and thus makes such a procedure impractical on classical computers for large systems. In most applications, only the second-order H_{eff} [28] is considered.

Quantum computation has attracted much attention in recent years. It has been proved that quantum computers are capable of handling problems which are intractable for classical computers [29,30]. While the fault-tolerant universal quantum computer [31,32] may not be feasible in the near term, noisy intermediate-scale quantum (NISQ) computers are possible candidates for applications in various fields including many-body quantum physics [33]. Starting with the variational quantum eigensolver (VQE) [34], which is a variational quantum algorithm [35], to estimate the ground state of a given Hamiltonian using shallow circuits, many useful quantum algorithms for NISQ computers have been proposed [36–39].

In this paper, we propose two quantum algorithms to realize SWT and obtain the effective Hamiltonian. The first algorithm constructs the unitary U directly using a quantum circuit under the observation that U is composed of two reflection operators acting on the unperturbed and perturbed Hamiltonians. The reflection operators effectively apply a phase flip to the high-energy eigenstates, and U additionally applies a conditional phase change to the state. This method makes use of the quantum phase estimation (QPE) algorithm to distinguish the states corresponding to low- and high-energy eigenspaces, and thus may require circuit depths exceeding the limits of hardware available in the NISQ era. Therefore, we propose the second algorithm for NISQ devices. It is a hybrid quantum-classical algorithm based on the variational algorithm. The cost function is designed such that it can reach the minimum when the evolution of a state within the low-energy subspace of the unperturbed Hamiltonian is independent of time. The parameterized cost function can be measured using a quantum computer, and the parameters are to be optimized with a classical algorithm. To demonstrate the

*xsxu@g scaep.ac.cn

†yli@g scaep.ac.cn

Published by the American Physical Society under the terms of the [Creative Commons Attribution 4.0 International](https://creativecommons.org/licenses/by/4.0/) license. Further distribution of this work must maintain attribution to the author(s) and the published article's title, journal citation, and DOI.

effectiveness of our second algorithm, we performed numerical simulations using QuESTlink [40] and *qasm_simulator* as well as experiments on the IBMQ quantum computer *ibmq_manila*, with the example of a four-qubit Heisenberg chain with long-distance entanglement between the two ends.

This paper is organized as follows. In Sec. II, we give a brief introduction to SWT. Next, in Secs. III and IV, we describe the two quantum algorithms to construct SWT, respectively. The proof-of-principle numerical simulations and experiments are presented in Sec. V. This paper ends with a conclusion in Sec. VI.

II. SCHRIEFFER-WOLFF TRANSFORMATION

In degenerate perturbation theory, we consider a Hamiltonian $H = H_0 + \epsilon V$, where H_0 is the unperturbed Hamiltonian with well-separated low- and high-energy levels, and ϵV is the perturbation which brings the split of the spectra. The SWT is a unitary transformation that maps the total Hamiltonian H to the low-energy effective Hamiltonian H_{eff} , which acts on the low-energy subspace of H_0 and reproduces the low-energy spectrum of H .

The unperturbed Hamiltonian H_0 can be written into low-energy and high-energy levels according to the spectral decomposition

$$H_0 = \sum_{i=1}^M E_i^{(0)} |\phi_i^{(0)}\rangle\langle\phi_i^{(0)}| + \sum_{i=M+1}^N E_i^{(0)} |\phi_i^{(0)}\rangle\langle\phi_i^{(0)}|, \quad (1)$$

with eigenvalues $E_1^{(0)} \leq \dots \leq E_M^{(0)} < E_{M+1}^{(0)} \leq \dots \leq E_N^{(0)}$. Here N is the dimension of the system's Hilbert space and M is the dimension of the low-energy eigenspace of H_0 , denoted as \mathcal{P}_0 . Define P_0 as the projector on \mathcal{P}_0 ,

$$P_0 = \sum_{i=1}^M |\phi_i^{(0)}\rangle\langle\phi_i^{(0)}|, \quad (2)$$

and $Q_0 = I - P_0$ is its complement.

The low-energy and high-energy spectra are separated by the gap:

$$\Delta = E_{M+1}^{(0)} - E_M^{(0)}. \quad (3)$$

It is assumed that ϵV is small and satisfies

$$\|\epsilon V\| < \frac{\Delta}{2}, \quad (4)$$

where $\|\cdot\|$ is the operator norm. Since the perturbation shifts the eigenvalues of H_0 by at most $\|\epsilon V\|$, there will still be a positive gap between the low-energy and the high-energy spectra.

So, the total Hamiltonian can be written as

$$H = \sum_{i=1}^M E_i |\phi_i\rangle\langle\phi_i| + \sum_{i=M+1}^N E_i |\phi_i\rangle\langle\phi_i|, \quad (5)$$

with its eigenvalues $E_1 \leq \dots \leq E_M < E_{M+1} \leq \dots \leq E_N$. Denote \mathcal{P} as the M -dimension low-energy eigenspace of H and define P as the projector on \mathcal{P} , then $Q = I - P$ is its complement. Thus the total Hamiltonian can be expressed as a block-diagonal form

$$H = PHP + QHQ. \quad (6)$$

P and P_0 can be connected with a unitary U ,

$$UPU^\dagger = P_0, \quad (7)$$

which is exactly the SWT. Likewise, we can find

$$UQU^\dagger = Q_0. \quad (8)$$

It has been proved in Ref. [6] that U can be constructed by reflection operators $R_{\mathcal{P}_0}$ and $R_{\mathcal{P}}$,

$$U = \sqrt{R_{\mathcal{P}_0} R_{\mathcal{P}}}, \quad (9)$$

where $R_{\mathcal{P}_0} = 2P_0 - I$ and $R_{\mathcal{P}} = 2P - I$. Note that in some places U is defined as $U = e^S$, where S is called the generator of the transformation [15,41].

Using Eqs. (6)–(8), the transformed Hamiltonian H' can be reexpressed as [42]

$$\begin{aligned} H' &= UHU^\dagger \\ &= UPHPU^\dagger + UQHQU^\dagger \\ &= P_0UHU^\dagger P_0 + Q_0UHU^\dagger Q_0, \end{aligned} \quad (10)$$

which indicates that H' is block-diagonal with respect to P_0 and Q_0 . Project H' onto \mathcal{P}_0 yields the low-energy effective Hamiltonian

$$H_{\text{eff}} = P_0UHU^\dagger P_0, \quad (11)$$

whose M eigenvalues are the same as the M lowest eigenvalues of H .

To obtain H_{eff} , one needs to find U . In the following, we propose two quantum algorithms to find H_{eff} . The first algorithm is for universal fault-tolerant quantum computers and the second one is a hybrid approach based on the variational approach and thus is suitable for near-term quantum devices.

III. THE QUANTUM ALGORITHM FOR SWT

In many models, the Hamiltonian H can be decomposed into Pauli terms

$$H = \sum_{i=1}^{N_h} h_i \sigma_i, \quad (12)$$

and the term number N_h increases polynomially with the system size n , e.g., the Heisenberg model and Fermi-Hubbard model [43]. For each σ_i , we can construct a density matrix $\rho_i = (\sigma_i + \mathbb{1})/2^n$, thus $\sigma_i = 2^n \rho_i - \mathbb{1}$. Then, the effective Hamiltonian in Eq. (11) becomes

$$H_{\text{eff}} = \sum_{i=1}^{N_h} h_i (2^n P_0 U \rho_i U^\dagger P_0 - P_0). \quad (13)$$

Notice that ρ_i is a quantum state which can be prepared with a quantum computer, the idea is to apply U to the state, perform projective measurement onto P_0 , and then obtain $P_0 U \rho_i U^\dagger P_0$ (by postselection according to the measurement result). For large systems, ρ_i is highly mixed and can be realized with the Monte Carlo method. For instance, for $\sigma_i^z = Z \otimes I^{\otimes(n-1)}$, $\rho_i^z = (\sigma_i^z + \mathbb{1})/2^n = |0\rangle\langle 0| \otimes (I/2)^{\otimes(n-1)}$. This state can be sampled by initializing the first qubit in $|0\rangle$ and the others in $|0\rangle$ or $|1\rangle$ with equal probability. For a general Pauli operator σ_i , we can find a unitary V that satisfies $\sigma_i = V \sigma_i^z V^\dagger$, thus

we have $\rho_i = V \rho_1^z V^\dagger$, which can be efficiently sampled with a variance $\propto \frac{1}{N_s}$, where N_s is the number of sampling times. The full tomography of each $P_0 U \rho_i U^\dagger P_0$ is unrealistic when the system size is large, therefore we need an ansatz of the effective Hamiltonian $H_{\text{eff}} = \sum_{\tau \in A} g_\tau \tau$. Here A is a subset of Pauli operators that can be generated with prior knowledge of H based on perturbation theory [44–48], renormalization [49–51], etc. Then,

$$g_\tau = \sum_{i=1}^{N_h} h_i [\text{Tr}(\tau P_0 U \rho_i U^\dagger P_0) - 2^{-n} \text{Tr}(\tau P_0)], \quad (14)$$

where n is the qubit number. In general, we can realize the projective measurement onto P_0 using QPE [52]: We use QPE to measure the eigenenergy of the unperturbed Hamiltonian, but the final measurement is adapted for distinguishing two subspaces P_0 and Q_0 instead of specific eigenenergies. The total number of expected values evaluated for constructing H_{eff} is $N_h \times |A|$. Therefore, by taking an ansatz in which $|A|$ is polynomial, the overall cost for reconstructing H_{eff} is polynomial. Next, we show that U is equivalent to an oracle which does conditional phase rotations to some states.

Given an arbitrary state, it can be written in the basis of the eigenspace of H ,

$$|\Psi\rangle = \sum_{i=1}^N \alpha_i |\phi_i\rangle, \quad (15)$$

thus $e^{iH} |\Psi\rangle = \sum_{i=1}^N \alpha_i e^{iE_i} |\phi_i\rangle$. As $R_{\mathcal{D}} = 2P - I$ and P is the projector on the low-energy eigenspace, $R_{\mathcal{D}}$ is effectively a reflection operator that does a phase flip to the eigenstates corresponding to the high-energy space, namely,

$$R_{\mathcal{D}} |\Psi\rangle = \sum_{i=1}^M \alpha_i |\phi_i\rangle - \sum_{i=M+1}^N \alpha_i |\phi_i\rangle. \quad (16)$$

The same applies for $R_{\mathcal{D}_0}$.

On a quantum computer, we could use QPE to realize the unitary operator $R_{\mathcal{D}}$,

$$\begin{aligned} |+\rangle^{\otimes l} \otimes |\Psi\rangle &= \frac{1}{\sqrt{2^l}} \sum_{x=0}^{2^l-1} |x\rangle \otimes \sum_{i=1}^N \alpha_i |\phi_i\rangle \\ &\xrightarrow{U_{\text{QPE}}} \sum_{i=1}^N \alpha_i \sum_{k=0}^{2^l-1} f_i(k) |k\rangle \otimes |\phi_i\rangle, \end{aligned} \quad (17)$$

where l is the number of ancilla qubits, $U_{\text{QPE}} = \sum_{x=0}^{2^l-1} |x\rangle \langle x| \otimes e^{-iHt x}$, t is chosen such that eigenvalues of Ht are within the interval $[0, 2\pi)$, and $f_i(k) = \frac{1}{2^l} \sum_{x=0}^{2^l-1} e^{i(\frac{2\pi k}{2^l} - E_i t)x}$. As the amplitude $f_i(k)$ is concentrated at $k \simeq \frac{2^l E_i t}{2\pi}$, we could make a phase flip to the states with $E_i > E_M^{(0)} + \Delta/2$, by applying the unitary gate $\sum_{k=0}^{k_{th}-1} |k\rangle \langle k| - \sum_{k=k_{th}}^{2^l-1} |k\rangle \langle k|$ on ancilla qubits, where $k_{th} = \lceil \frac{2^l (E_M^{(0)} + \Delta/2) t}{2\pi} \rceil$. Then we apply U_{QPE}^{-1} to get

$$\frac{1}{\sqrt{2^l}} \sum_{x=0}^{2^l-1} |x\rangle \otimes \left(\sum_{i=1}^M \alpha_i |\phi_i\rangle - \sum_{i=M+1}^N \alpha_i |\phi_i\rangle \right) \quad (18)$$

up to a small error due to the finite resolution of QPE (i.e., 2^l is finite). Performing Hadamard transform and measuring the ancilla qubits with result $|0\rangle^{\otimes l}$, we get Eq. (16). We then apply $R_{\mathcal{D}_0}$ to $R_{\mathcal{D}} |\Psi\rangle$ to get $R_{\mathcal{D}_0} R_{\mathcal{D}} |\Psi\rangle$.

As $U = \sqrt{R_{\mathcal{D}_0} R_{\mathcal{D}}}$, if eigenvalues and eigenvectors of $R_{\mathcal{D}_0} R_{\mathcal{D}}$ are $e^{i\theta_j}$ and $|\psi_j\rangle$, i.e.,

$$R_{\mathcal{D}_0} R_{\mathcal{D}} |\Psi\rangle = \sum_j \beta_j e^{i\theta_j} |\psi_j\rangle, \quad (19)$$

we have

$$U |\Psi\rangle = \sum_j \beta_j e^{i\frac{\theta_j}{2}} |\psi_j\rangle. \quad (20)$$

Here, an arbitrary state $|\Psi\rangle$ is written in eigenvectors of the double reflection operator. Therefore, we could use QPE to realize the phase $e^{i\frac{\theta_j}{2}}$:

$$\begin{aligned} |+\rangle^{\otimes m} \otimes |\Psi\rangle &= \frac{1}{\sqrt{2^m}} \sum_{x=0}^{2^m-1} |x\rangle \otimes \sum_j \beta_j |\psi_j\rangle \\ &\xrightarrow{U'_{\text{QPE}}} \sum_j \beta_j \sum_{k=0}^{2^m-1} g_j(k) |k\rangle \otimes |\psi_j\rangle, \end{aligned} \quad (21)$$

where m is the number of ancilla qubits, $U'_{\text{QPE}} = \sum_{x=0}^{2^m-1} |x\rangle \langle x| \otimes (R_{\mathcal{D}_0} R_{\mathcal{D}})^x$ and $g_j(k) = \frac{1}{2^m} \sum_{x=0}^{2^m-1} e^{i(\frac{2\pi k}{2^m} + \theta_j)x}$. Because $g_j(k)$ is concentrated at $k \simeq -\frac{2^m \theta_j}{2\pi}$, the phase θ_j is (approximately) stored on the ancilla qubits. We then apply the phase gate $\sum_{k=0}^{2^m-1} e^{-i\frac{\pi k}{2^m}} |k\rangle \langle k|$ before applying U'_{QPE} . Therefore, the overall effect of all these steps applies a phase of $e^{i\frac{\theta_j}{2}}$ to the state $|\psi_j\rangle$ and thus effectively realizes $U |\Psi\rangle$.

To summarize, the whole procedure of this algorithm consists of two phases to realize $U |\Psi\rangle$: first, applying $R_{\mathcal{D}}$ ($R_{\mathcal{D}_0}$) to a state and then U , which can be implemented with quantum circuits of the same structure. The pseudocodes and the quantum circuit can be found in Appendix A. This algorithm has a gate complexity of $O(2^m(2^l N_t + l^2) + m^2)$, where N_t is the number of gates in the Trotterization, with details also given in Appendix A. We define the error of this algorithm as the 2-norm between the ideal and actual states. The total error ϵ_{tot} is estimated as $2^{m+2}(2^{l+1}\epsilon_t + \epsilon_l) + \epsilon_m$, where ϵ_t is the error of Trotterization, ϵ_l is $O(1/\sqrt{2^l}(E_{M+1} - E_M)t)$, and ϵ_m is $O(2^{-m/2})$. ϵ_{tot} can decrease exponentially with the number of ancilla qubits, and to control the error we need to take $l > 2m$. The detailed error analysis can be found in Appendix B.

As this algorithm needs to apply a concatenated QPE, which uses deep circuits and a reasonable number of ancilla qubits for high resolutions of energy and phase, it is not feasible until large-scale error-protected quantum computers come to exist. In the next section, we introduce a hybrid algorithm which is suitable for near-term quantum devices.

IV. THE HYBRID QUANTUM-CLASSICAL ALGORITHM FOR SWT

If UHU^\dagger is block diagonal with respect to P_0 and Q_0 , we can infer that H is block diagonal with respect to P and

Q , where $P = U^\dagger P_0 U$ and $Q = U^\dagger Q_0 U$ are projectors transformed by inverse SWT. Under this condition, a state within the subspace of \mathcal{P} should remain in the subspace as it evolves. Therefore, we can design a cost function as the following:

$$\mathcal{L}_t(\vec{\theta}) = -\frac{1}{M} \sum_{i,j}^M |\langle \phi_i^{(0)} | U(\vec{\theta}) e^{-iHt} U^\dagger(\vec{\theta}) | \phi_j^{(0)} \rangle|^2, \quad (22)$$

where $|\phi_i^{(0)}\rangle$ and $|\phi_j^{(0)}\rangle$ are the basis states in \mathcal{P}_0 and $U(\vec{\theta})$ is constructed by a parameterized quantum circuit. We remark that we can use the Monte Carlo method to evaluate the cost function rather than measure each term in it. We find the global minimum of the cost function $\mathcal{L}_{t,\min}$ is -1 , obtained when H is block diagonal with respect to P and Q , i.e., $U(\vec{\theta})$ is exactly the unitary transformation U that realizes the SWT. However, to minimize this cost function using a quantum computer, one needs to implement e^{-iHt} , which usually requires deep circuits to achieve high accuracy.

Now we introduce an alternative cost function. When $U(\vec{\theta}) = U$, $\mathcal{L}_{t,\min} = -1$, and thus is invariant when the time t changes. Therefore, we rewrite \mathcal{L}_t in the form of a Taylor series about t :

$$\mathcal{L}_t = A + Bt + Ct^2 + Dt^3 + \dots \quad (23)$$

Extracting the coefficients A , B , and C , we have

$$A = -1, \quad (24)$$

$$B = 0, \quad (25)$$

$$C = \frac{1}{M} \left(\sum_{i=1}^M \langle \phi_i^{(0)} | U(\vec{\theta}) H^2 U^\dagger(\vec{\theta}) | \phi_i^{(0)} \rangle - \sum_{i,j}^M |\langle \phi_i^{(0)} | U(\vec{\theta}) H U^\dagger(\vec{\theta}) | \phi_j^{(0)} \rangle|^2 \right). \quad (26)$$

The derivation is given in Appendix C. When $U(\vec{\theta}) = U$, because $\mathcal{L}_{t,\min}$ is time independent, all the coefficients except A must be 0.

In fact, we find that when $C = 0$, $\mathcal{L}_t = -1$ exactly holds for all t , which means the effective model is exact. Technically, $C = 0$ is equivalent to the complete block diagonalization of H with respect to P and Q . The proof can be found in Appendix D. It implies that if $C = 0$, the coefficients of the higher order Taylor series must also be 0. Therefore, if there exists $U(\vec{\theta}_{\text{opt}})$ such that $C = 0$, we know $U(\vec{\theta}_{\text{opt}}) = U$. With this, we can reconstruct the cost function as the absolute value of C ,

$$\begin{aligned} \mathcal{L}(\vec{\theta}) &= |C| \\ &= \frac{1}{M} \left| \sum_{i=1}^M \langle \phi_i^{(0)} | U(\vec{\theta}) H^2 U^\dagger(\vec{\theta}) | \phi_i^{(0)} \rangle - \sum_{i,j}^M |\langle \phi_i^{(0)} | U(\vec{\theta}) H U^\dagger(\vec{\theta}) | \phi_j^{(0)} \rangle|^2 \right|, \quad (27) \end{aligned}$$

which has the global minimum 0. Note that we make $\mathcal{L}(\vec{\theta})$ the absolute value of C to avoid the case where it becomes negative with experimental noise.

Now we have the final version of the cost function. Starting from an initial parameter set $\vec{\theta}_0$, our hybrid algorithm optimizes the set $\vec{\theta}$ such that $\mathcal{L}(\vec{\theta})$ reaches minimum after several iteration cycles. In each cycle, $\mathcal{L}(\vec{\theta})$ is measured using a quantum computer, and a classical algorithm is used to optimize $\vec{\theta}$ based on $\mathcal{L}(\vec{\theta})$. The iteration continues until $\mathcal{L}(\vec{\theta})$ reaches its minimum. Then we obtain the corresponding $U(\vec{\theta})$ as a good approximation of U .

To implement the hybrid algorithm, the basis set $\{|\phi_i^{(0)}\rangle\}$ of the unperturbed Hamiltonian H_0 must be known. The Hamiltonian H is decomposed into Pauli terms $H = \sum_l h_l \sigma^l$, thus $\mathcal{L}(\vec{\theta})$ has $O(N_h M)$ terms and each term has the form $\langle \phi_i^{(0)} | U(\vec{\theta}) \sigma^l U^\dagger(\vec{\theta}) | \phi_j^{(0)} \rangle$, which can be measured using a quantum computer [53,54]. In the following section, we demonstrate the hybrid algorithm using an example of a one-dimensional Heisenberg model.

V. SIMULATION AND EXPERIMENT

We demonstrate the effectiveness of the hybrid algorithm with experiments on an IBMQ quantum device. We choose a spin model to verify our methods in Sec. IV. The system is an antiferromagnetic Heisenberg chain with modulated interaction strengths [55]. Two spins at the ends of the chain are weakly coupled to other spins on the chain. If the chain with two ends removed has a nondegenerate ground state and an energy gap above the ground state, two end spins are effectively coupled through the chain: According to the perturbation theory, two end spins are directly coupled in the effective model. We will reconstruct the effective model of the Heisenberg chain with experiments on IBMQ devices.

A. Model

The unperturbed Hamiltonian is the chain with two end spins decoupled, i.e.,

$$H_0 = 2 \sum_{i=2}^{N-2} (\sigma_i^x \sigma_{i+1}^x + \sigma_i^y \sigma_{i+1}^y + \sigma_i^z \sigma_{i+1}^z), \quad (28)$$

where N is the total number of spins. The perturbation is the interaction between end spins and the rest of the chain, i.e.,

$$\begin{aligned} V &= \sigma_1^x \sigma_2^x + \sigma_1^y \sigma_2^y + \sigma_1^z \sigma_2^z \\ &+ \sigma_{N-1}^x \sigma_N^x + \sigma_{N-1}^y \sigma_N^y + \sigma_{N-1}^z \sigma_N^z. \quad (29) \end{aligned}$$

Thinking that end spins 1 and N are removed from the system, the Hamiltonian of spins 2 to $N-1$ is H_0 . Then, if the ground state of H_0 (without considering spins 1 and N) is nondegenerate, the unperturbed ground-state subspace of all spins is fourfold degenerate. Let $|\text{GS}\rangle$ be a state of spins 2 to $N-1$ and the nondegenerate ground state of H_0 , the ground-state subspace of all spins has the basis $\{|\mu\rangle \otimes |\text{GS}\rangle \otimes |\nu\rangle \mid \mu, \nu = 0, 1\}$. If $N = 4$, the subsystem ground state is the singlet state $|\text{GS}\rangle = \frac{1}{\sqrt{2}}(|0\rangle \otimes |1\rangle - |1\rangle \otimes |0\rangle)$; in general, we can obtain the ground state $|\text{GS}\rangle$ via VQE.

With perturbation, usually the ground state splits into singlet ground state and triplet excited states because of the symmetry of the Heisenberg interaction. So, the effective Hamiltonian acting in this low-energy subspace is equivalent to Heisenberg interaction between spins 1 and N . The effective ground state of the subspace of spins 1 and N is then $\frac{1}{\sqrt{2}}(|01\rangle_{1,N} - |10\rangle_{1,N})$. The entanglement between two separated spins comes from repeated nearest-neighbor interactions in the Heisenberg chain.

B. Ansatz

Here we adopt an empirical ansatz to construct the transformation U . If H_0 and V commute, they are simultaneously (block) diagonalizable by a unitary transformation, and U is identity. So this commutative situation is trivial. If H_0 and V do not commute, we can express the commutator as a linear combination of Pauli operators,

$$[H_0, V] = i \sum_{j=1}^M \alpha_j \sigma^{(j)}, \quad (30)$$

where α_j is a real scalar coefficient. Note that usually the number of Pauli operators M in the linear combination increases polynomially with the system size. Given the commutator, we approximate the generator S with an operator in the form [41]

$$\eta = \sum_{j=1}^M \eta_j \sigma^{(j)}. \quad (31)$$

Supposing coefficients η_j are small, we can approximate $U = e^S$ with the ansatz transformation

$$U(\vec{\theta}) = \prod_{j=1}^M e^{i\sigma^{(j)}\theta_j}, \quad (32)$$

where parameters θ_j are optimized according to our algorithm in Sec. IV.

Taking $N = 4$ in the model, we find that U has 12 terms. By removing parameters that have little impact on the cost function, U is simplified to six terms to reduce circuit depth. Considering the symmetry of the system, we keep three parameters. Finally, the ansatz is

$$U(\vec{\theta}) = e^{i\sigma_2^z \sigma_3^y \sigma_4^x \theta_1/2} e^{i\sigma_2^z \sigma_3^x \sigma_4^y \theta_2/2} e^{i\sigma_2^y \sigma_3^z \sigma_4^x \theta_3/2} e^{i\sigma_1^z \sigma_2^x \sigma_3^y \theta_3/2} e^{i\sigma_1^y \sigma_2^z \sigma_3^x \theta_2/2} e^{i\sigma_1^x \sigma_2^y \sigma_3^z \theta_1/2}, \quad (33)$$

and the corresponding circuit is drawn as Fig. 5 in Appendix A.

C. Measurement circuits

As mentioned before, one needs to measure the transition amplitude $\langle \phi_i^{(0)} | U(\vec{\theta}) \sigma^l U^\dagger(\vec{\theta}) | \phi_j^{(0)} \rangle$, where $|\phi_j^{(0)}\rangle$ is one of the four basis states of the ground-state subspace. We can measure the transition amplitude using a Hadamard test circuit [53]. To minimize the gate number, which is important in NISQ devices, we measure the transition amplitude in the following way. We consider two cases. In the first case, when $i = j$, the transition amplitude is the expected value of σ^l in the state $U^\dagger(\vec{\theta})|\phi_j^{(0)}\rangle$, which can be directly measured: We prepare the state $|\phi_j^{(0)}\rangle$, then apply the transformation $U^\dagger(\vec{\theta})$ and finally

TABLE I. All possible combinations of $|\phi_i^{(0)}\rangle$ and G . $|\Phi\rangle \equiv |0\rangle \otimes |\text{GS}\rangle \otimes |0\rangle$

$\langle \phi_i^{(0)} $	$ \phi_j^{(0)}\rangle$	G
$\langle \Phi $	$\sigma_1^x \Phi\rangle$	σ_1^x
$\langle \Phi $	$\sigma_N^x \Phi\rangle$	σ_N^x
$\langle \Phi $	$\sigma_1^x \sigma_N^x \Phi\rangle$	$\sigma_1^x \sigma_N^x$
$\langle \Phi \sigma_1^x$	$\sigma_N^x \Phi\rangle$	$\sigma_1^x \sigma_N^x$
$\langle \Phi \sigma_1^x$	$\sigma_1^x \sigma_N^x \Phi\rangle$	σ_N^x
$\langle \Phi \sigma_N^x$	$\sigma_1^x \sigma_N^x \Phi\rangle$	σ_1^x

measure σ^l . In the second case, when $i \neq j$, we always have $|\phi_j^{(0)}\rangle = G|\phi_i^{(0)}\rangle$, where $G = \mathbb{1}, \sigma_1^x, \sigma_N^x, \sigma_1^x \sigma_N^x$. Then the transition amplitude becomes

$$\begin{aligned} & \langle \phi_i^{(0)} | U(\vec{\theta}) \sigma^l U^\dagger(\vec{\theta}) | \phi_j^{(0)} \rangle \\ &= \langle \phi_i^{(0)} | U(\vec{\theta}) \sigma^l U^\dagger(\vec{\theta}) G | \phi_i^{(0)} \rangle \\ &= \langle \phi_i^{(0)} | \frac{I+G}{2} U(\vec{\theta}) \sigma^l U^\dagger(\vec{\theta}) \frac{I+G}{2} | \phi_i^{(0)} \rangle \\ &\quad - \langle \phi_i^{(0)} | \frac{I-G}{2} U(\vec{\theta}) \sigma^l U^\dagger(\vec{\theta}) \frac{I-G}{2} | \phi_i^{(0)} \rangle \\ &\quad - i \langle \phi_i^{(0)} | \frac{I-iG}{2} U(\vec{\theta}) \sigma^l U^\dagger(\vec{\theta}) \frac{I+iG}{2} | \phi_i^{(0)} \rangle \\ &\quad + i \langle \phi_i^{(0)} | \frac{I+iG}{2} U(\vec{\theta}) \sigma^l U^\dagger(\vec{\theta}) \frac{I-iG}{2} | \phi_i^{(0)} \rangle. \end{aligned} \quad (34)$$

According to the above equation, the transition amplitude becomes a linear combination of expected values of σ^l in states $\frac{I \pm G}{2} |\phi_i^{(0)}\rangle$ and $\frac{I \pm iG}{2} |\phi_i^{(0)}\rangle$ [54]. We can measure these expected values by preparing these four states (up to the normalization factor). In our case, because the transition amplitude is always real, we only need to prepare states $\frac{I \pm G}{2} |\phi_i^{(0)}\rangle$. See Table I for combinations of $|\phi_i^{(0)}\rangle$ and G .

D. Implementation and results

Now we demonstrate our algorithm on an IBM quantum device *ibmq_manila*, a five-qubit superconducting quantum computer with readout error rates 2.02% ~ 3.53%, single-qubit gate error rates 0.02% ~ 0.03%, and CNOT gate error rates 0.55% ~ 1.23% during our experiments.

In each experiment, the initial parameter vector $\vec{\theta}_0$ was set to zero and the SPSA [56] algorithm was used to optimize parameters in each cycle of the iteration. The optimization process continued until the cost function stopped declining in several successive iterations. During the experiment, the Clifford data regression (CDR) error mitigation technique [57], which is a simplified version of Clifford data learning [58], was used to improve the result. Each circuit was run for 10^4 shots.

The amplitudes obtained in quantum computer were used to construct H_{eff} . This is equivalent to the full tomography of each $U \sigma^l U^\dagger$ in the subspace P_0 . In this experiment, H_{eff} is a 4×4 matrix with the element in row i and column j given by $\langle \phi_i^{(0)} | U(\vec{\theta}) H U^\dagger(\vec{\theta}) | \phi_j^{(0)} \rangle$, which is also used to evaluate the cost function. With H_{eff} , one can use the VQE approach to compute the low-energy spectra. However, considering the

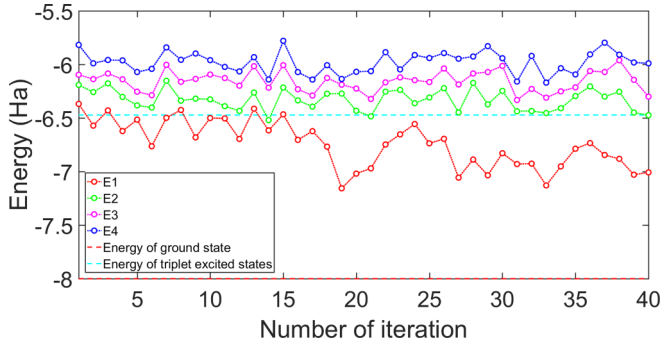


FIG. 1. Eigenvalues of H_{eff} experimentally measured using experimentally obtained parameters.

case that the dimension of H_{eff} is far less than H , we may be able to efficiently diagonalize H_{eff} to obtain the spectrum. In this work we simply diagonalize H_{eff} using a classical computer.

The results are shown in Fig. 1. As the iteration goes, the energies of the four eigenstates gradually approach the correct values with significant fluctuations. This is largely attributed to the high read out error of the quantum device, as can be supported by Fig. 2, where we classically compute the effective energy using the same set of parameters. We see smoother curves and the results are more close to the exact values.

We summarize the results in Fig. 3, where we show the final energies obtained from both numerical simulations and experiments. The numerical simulations in the noise-free case were conducted using QuESTlink [40], a packaged quantum emulator, and a noisy case was considered and simulated using *qasm_simulator*. The fidelity of the low-energy states with respect to the exact reference state, calculated by diagonalization of H_{eff} in each case, is reflected as the color of each short line.

One thing needed to be noted is that to reduce the circuit depth, we use a simple ansatz which can well approximate the exact reference states but is not a perfect choice. As can be seen from the second column in Fig. 3, there is a small gap between the exact solutions and the simulated results. Better results are expected with a more complex ansatz.

In addition, the error mitigation technique relies on a good estimation of the noise. The CDR approach estimates the error

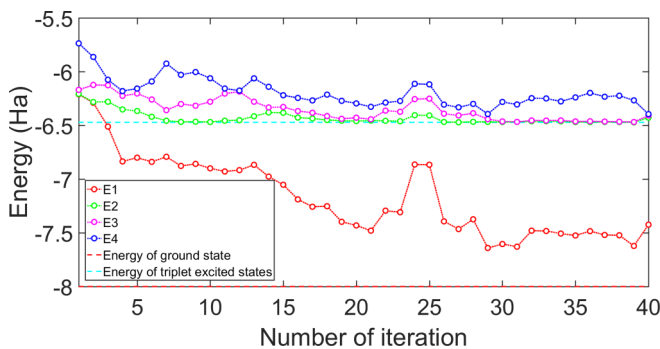


FIG. 2. Eigenvalues of H_{eff} classically computed using experimentally obtained parameters.

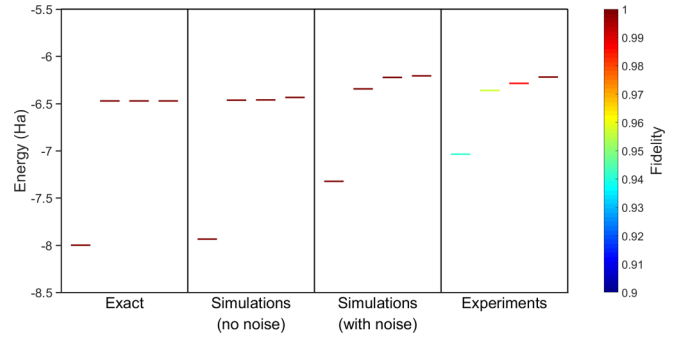


FIG. 3. The final energies in the low-energy spectrum and the fidelity of the obtained states with respect to the exact solutions. From left to right: Exact energies, results from simulations with no noise, simulations with noise model from *ibmq_manila*, and experiments on *ibmq_manila*. Horizontal solid line shows the energy value, with color indicating the fidelity with respect to the corresponding reference state.

information by measuring a set of observables using a circuit very close to the original one but with only Clifford gates. On IBMQ, circuits are running in batches, so we performed CDR circuits once in each batch. During the experiment, however, the error fluctuates and deviates from the calibrated data and thus weakens the effect of error mitigation. The third column in Fig. 3 shows the final energies obtained from numerical simulations on *qasm_simulator* with a simplified noise model generated from the real-time calibration information of the *ibmq_manila* device (a function provided by IBMQ). Error mitigation was performed where the error information comes directly from the real-time calibration data. We see that with a better description of the error model, error mitigation performs better and the final results are more close to the exact values.

VI. DISCUSSION AND CONCLUSION

In this paper, we proposed two quantum algorithms to realize the SWT. The first algorithm constructs the SWT using a quantum circuit and evaluates the effective Hamiltonian with projection measurement. This method scales polynomially with the problem size and is suitable for fault-tolerant quantum computers. The second algorithm is a hybrid algorithm applicable to NISQ devices. This method is based on the variational algorithm, but instead of constructing a cost function to minimize the energy, our cost function is derived by using the block diagonalization property of the Hamiltonian. By optimizing the parameters, the cost function gradually approaches zero and the effective Hamiltonian can be obtained directly from the elements of the cost function. To verify this algorithm, we implemented it numerically and on an IBM quantum device using the example of a Heisenberg chain model with long-distance entanglement. The simulated results are very close to the exact values, and on a noisy device, we obtain the final states with over 95% fidelity. To improve the results, some delicately designed error mitigation techniques can be applied.

Note that this method is not limited to finding the ground-state energy of a many-body system but is able to find any

energy interval of interest as long as they have no energy-level crossings with others under perturbation. The interested readers can refer to Appendix E for a generalized description.

ACKNOWLEDGMENTS

We thank Dayue Qin for discussions. We acknowledge the use of simulation toolkit QuESTlink [40] and IBM Quantum services [59] for this work. We acknowledge the support of the National Natural Science Foundation of China (Grants No. 11875050 and No. 12088101) and NSAF (Grant No. U1930403).

APPENDIX A: THE QUANTUM CIRCUITS FOR THE TWO ALGORITHMS AND PSEUDO CODES FOR THE FAULT-TOLERANT ALGORITHM

Let $C_a(V^{2^{a-1}})$ be a controlled-V gate with the a th ancilla qubit as the control qubit. The pseudo codes are given in Tables II and III.

The quantum circuit of the procedure is shown in Fig. 4. The gate complexities are listed in Table IV.

Figure 5 shows the quantum circuit used in our hybrid quantum-classical algorithm.

APPENDIX B: ERROR ANALYSIS FOR THE FAULT-TOLERANT ALGORITHM

Let $|a\rangle$ be the ideal state and $|b\rangle$ be the actual state. Define $\epsilon = \||a\rangle - |b\rangle\|$ as the error, where $\|\cdot\|$ is the 2-norm. It is easy to see that ϵ is invariant under unitary transformations. Besides, ϵ is additive, i.e., the total error can be upper bounded by the sum of errors through the whole process.

1. The error in realizing the reflection operator

For $R_{\mathcal{D}}$, the controlled unitary gate is e^{-iHt} . Using the Trotterization, we can realize U_t such that $\|U_t - e^{-iHt}\| = \epsilon_t$, where $\epsilon_t \leq \frac{\|H\|^2 t^2}{2n_T}$ for the first-order Trotterization [60]. Therefore, $\|(U_t - e^{-iHt})|\Psi\rangle\| \leq \epsilon_t$, which is estimated as $O(\frac{\|H\|^2 t^2}{n_T})$.

Next, assuming the time evolution e^{-iHt} is exact, we consider the error ϵ_l between the actual state and the ideal state of the whole system (including data qubits and ancilla qubits) without projective measurement, which includes the error of states with ancilla qubits in $|0\rangle^{\otimes l}$ and the failure probability, i.e., the measurement result of ancilla qubits is not $|0\rangle^{\otimes l}$. Owing to the invariance under unitary transformations, the

TABLE II. Quantum algorithm for realizing $R_{\mathcal{D}}|\Psi\rangle$.

1: Input arbitrary state $ \Psi\rangle$, l ancilla qubits initialized to $ 0\rangle$, $V = e^{-iHt}$, $k_{th} = \lceil \frac{2^l(E_M^{(0)} + \Delta/2)t}{2\pi} \rceil$.	
2: $ 0\rangle^{\otimes l} \Psi\rangle$	▷ Initial state.
3: $\rightarrow \frac{1}{\sqrt{2^l}} \sum_{x=0}^{2^l-1} x\rangle \otimes \Psi\rangle$	▷ Hadamard transform.
4: $\rightarrow \frac{1}{\sqrt{2^l}} \sum_{x=0}^{2^l-1} x\rangle \otimes V^x \sum_{i=1}^N \alpha_i \phi_i\rangle$ $= \sum_{i=1}^N \alpha_i \frac{1}{\sqrt{2^l}} \sum_{x=0}^{2^l-1} x\rangle \otimes e^{-iE_i t x} \phi_i\rangle$	▷ Apply $C_a(V^{2^{a-1}})$ ($a = 1, \dots, l$) gates.
5: $\rightarrow \sum_{i=1}^N \alpha_i \frac{1}{\sqrt{2^l}} \sum_{x=0}^{2^l-1} (\sum_{k=0}^{2^l-1} \frac{1}{\sqrt{2^l}} e^{j\frac{2\pi xk}{2^l}} k\rangle) \otimes e^{-iE_i t x} \phi_i\rangle$ $= \sum_{i=1}^N \alpha_i \sum_{k=0}^{2^l-1} f_i(k) k\rangle \otimes \phi_i\rangle$	▷ Quantum Fourier transform.
6: $\rightarrow \sum_{i=1}^M \alpha_i \sum_{k=0}^{2^l-1} f_i(k) k\rangle \otimes \phi_i\rangle - \sum_{i=M+1}^N \alpha_i \sum_{k=0}^{2^l-1} f_i(k) k\rangle \otimes \phi_i\rangle$	▷ Apply gate $\sum_{k=0}^{k_h-1} k\rangle\langle k - \sum_{k=k_h}^{2^l-1} k\rangle\langle k $ on ancilla qubits.
7: $\rightarrow \frac{1}{\sqrt{2^l}} \sum_{x=0}^{2^l-1} x\rangle \otimes V^x (\sum_{i=1}^M \alpha_i \phi_i\rangle - \sum_{i=M+1}^N \alpha_i \phi_i\rangle)$	▷ Inverse quantum Fourier transform.
8: $\rightarrow \frac{1}{\sqrt{2^l}} \sum_{x=0}^{2^l-1} x\rangle \otimes (\sum_{i=1}^M \alpha_i \phi_i\rangle - \sum_{i=M+1}^N \alpha_i \phi_i\rangle)$	▷ Apply $C_a(V^{2^{a-1}})$ ($a = 1, \dots, l$) gates.
9: $\rightarrow 0\rangle^{\otimes l} \otimes (\sum_{i=1}^M \alpha_i \phi_i\rangle - \sum_{i=M+1}^N \alpha_i \phi_i\rangle)$	▷ Hadamard transform.
10: $\rightarrow \sum_{i=1}^M \alpha_i \phi_i\rangle - \sum_{i=M+1}^N \alpha_i \phi_i\rangle$	▷ Measure the ancilla qubits with result $ 0\rangle^{\otimes l}$.
11: Output $R_{\mathcal{D}} \Psi\rangle = \sum_{i=1}^M \alpha_i \phi_i\rangle - \sum_{i=M+1}^N \alpha_i \phi_i\rangle$.	

TABLE III. Quantum algorithm for realizing SWT.

1: Input arbitrary state $ \Psi\rangle$, m ancilla qubits initialized to $ 0\rangle$, $V = R_{\mathcal{D}_0}R_{\mathcal{D}}$.	
2: $ 0\rangle^{\otimes m} \Psi\rangle$	▷ Initial state.
3: $\rightarrow \frac{1}{\sqrt{2^m}} \sum_{x=0}^{2^m-1} x\rangle \otimes \Psi\rangle$	▷ Hadamard transform.
4: $\rightarrow \frac{1}{\sqrt{2^m}} \sum_{x=0}^{2^m-1} x\rangle \otimes V^x \sum_j \beta_j \psi_j\rangle$ $= \sum_j \beta_j \frac{1}{\sqrt{2^m}} \sum_{x=0}^{2^m-1} x\rangle \otimes e^{i\theta_j x} \psi_j\rangle$	▷ Apply $C_a(V^{2^{a-1}})$ ($a = 1, \dots, m$) gates.
5: $\rightarrow \sum_j \beta_j \frac{1}{\sqrt{2^m}} \sum_{x=0}^{2^m-1} (\sum_{k=0}^{2^m-1} \frac{1}{\sqrt{2^m}} e^{i\frac{2\pi xk}{2^m}} k\rangle) \otimes e^{i\theta_j x} \psi_j\rangle$ $= \sum_j \beta_j \sum_{k=0}^{2^m-1} g_j(k) k\rangle \otimes \psi_j\rangle$	▷ Quantum Fourier transform.
6: $\rightarrow \sum_j \beta_j \sum_{k=0}^{2^m-1} g_j(k) k\rangle \otimes e^{i\frac{\theta_j k}{2^m}} \psi_j\rangle$	▷ Apply phase gate $\sum_{k=0}^{2^m-1} e^{-i\frac{\pi k}{2^m}} k\rangle\langle k $ on ancilla qubits.
7: $\rightarrow \frac{1}{\sqrt{2^m}} \sum_{x=0}^{2^m-1} x\rangle \otimes V^x \sum_j \beta_j e^{i\frac{\theta_j x}{2^m}} \psi_j\rangle$	▷ Inverse quantum Fourier transform.
8: $\rightarrow \frac{1}{\sqrt{2^m}} \sum_{x=0}^{2^m-1} x\rangle \otimes \sum_j \beta_j e^{i\frac{\theta_j x}{2^m}} \psi_j\rangle$	▷ Apply $C_a(V^{\dagger 2^{a-1}})$ ($a = 1, \dots, m$) gates.
9: $\rightarrow 0\rangle^{\otimes m} \otimes \sum_j \beta_j e^{i\frac{\theta_j}{2^m}} \psi_j\rangle$	▷ Hadamard transform .
10: $\rightarrow \sum_j \beta_j e^{i\frac{\theta_j}{2^m}} \psi_j\rangle$	▷ Measure the ancilla qubits with result $ 0\rangle^{\otimes m}$.
11: Output $U \Psi\rangle = \sum_j \beta_j e^{i\frac{\theta_j}{2^m}} \psi_j\rangle$.	

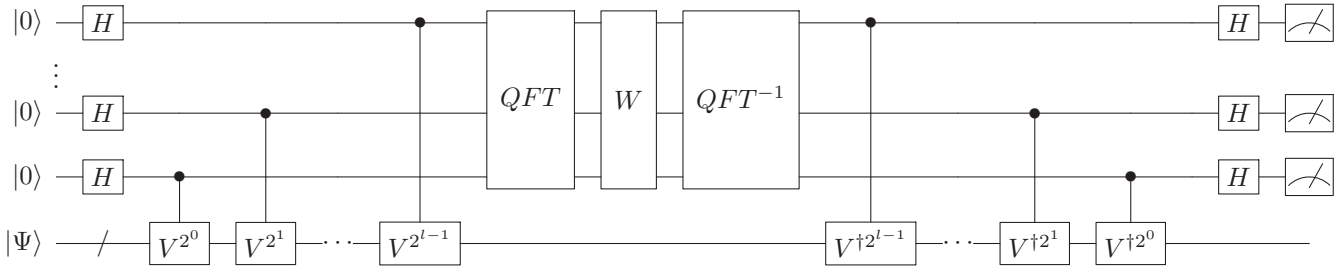


FIG. 4. The quantum circuit to realize $R_{\mathcal{D}}$ and U applying to a state $|\Psi\rangle$. To realize $R_{\mathcal{D}}$, $V = e^{-iHt}$ and the number of ancilla qubits is l . The W gate makes a phase flip for those $k \geq k_{th}$ ancilla qubit states $|k\rangle$, which is composed of at most l multiqubit controlled Z gates. To realize U , $V = R_{\mathcal{D}_0}R_{\mathcal{D}}$ and the number of ancilla qubits is m . The W gate applies a conditional phase $e^{-i\frac{\pi k}{2^m}}$ to $|k\rangle$, which is composed of m phase shift gates with phase shift $-\frac{\pi}{2^m} 2^{j-1}$ on the j th ancilla qubit.

TABLE IV. Gate counting. Here N_t is the number of gates in the Trotterization. We take the first-order Trotterization to realize the controlled- V when implementing R_p . Then N_t is $O(2nN_h n_T)$, where n_T is the trotter number.

	$R_{\mathcal{D}}$	U
Hadamard transform	l	m
Controlled- V	$O(2^l N_t)$	$O(2^m (2^l N_t + l^2))$
QFT	$O(l^2)$	$O(m^2)$
W	$\leq l$	m
QFT^{-1}	$O(l^2)$	$O(m^2)$
Controlled- V^\dagger	$O(2^l N_t)$	$O(2^m (2^l N_t + l^2))$
Hadamard transform	l	m
Total	$O(2^l N_t + l^2)$	$O(2^m (2^l N_t + l^2) + m^2)$

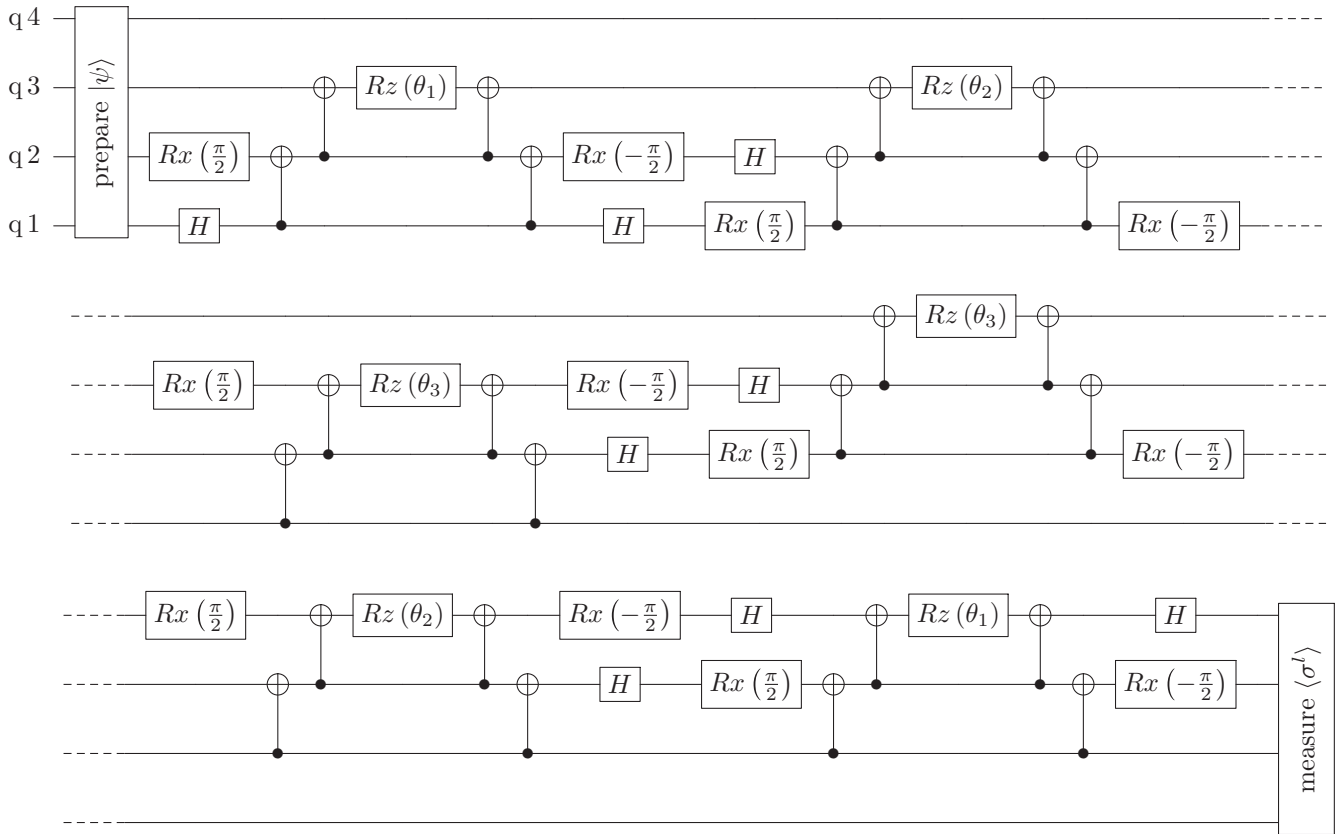


FIG. 5. The quantum circuit used in our experiments. In preparation, state $|\psi\rangle$ is $|\phi_i^{(0)}\rangle$ or $\frac{I \pm G}{2} |\phi_i^{(0)}\rangle$ (up to a normalization factor). In measurement, we measure the expectation of σ^l . The ansatz circuit is between these two blocks.

error between $|a\rangle$ and $|b\rangle$ in step 6 of Algorithm A is the same as that in step 9. Therefore,

$$|a\rangle \equiv \sum_{i=1}^M \alpha_i \sum_{k=0}^{2^l-1} f_i(k) |k\rangle \otimes |\phi_i\rangle - \sum_{i=M+1}^N \alpha_i \sum_{k=0}^{2^l-1} f_i(k) |k\rangle \otimes |\phi_i\rangle, \quad (B1)$$

$$|b\rangle \equiv \sum_{i=1}^N \alpha_i \left(\sum_{k=0}^{k_{ih}-1} f_i(k) |k\rangle - \sum_{k_{ih}}^{2^l-1} f_i(k) |k\rangle \right) \otimes |\phi_i\rangle, \quad (B2)$$

where l is the number of ancilla qubits and $f_i(k) = \frac{1}{2^l} \sum_{x=0}^{2^l-1} e^{i(\frac{2\pi k}{2^l} - E_i t)x}$.

For $M+1 \leq i \leq N$, $0 \leq E_i t < 2\pi$ and let $\frac{2\pi k_i}{2^l}$ be the best l bit approximation to $E_i t$ which is less than $E_i t$. The difference between $\frac{2\pi k_i}{2^l}$ and $E_i t$ satisfies $2\pi(\frac{k_i}{2^l} + \delta) = E_i t$ such that $0 \leq \delta < \frac{1}{2^l}$. Let $2\theta_k = \frac{2\pi k}{2^l} - E_i t = \frac{2\pi}{2^l}(k - k_i - 2^l \delta)$, when $-2^{l-1} < k - k_i \leq 2^{l-1}$ we have $-\frac{\pi}{2} < \theta_k < \frac{\pi}{2}$.

$$|f_i(k)|^2 = \left| \frac{1}{2^l} \frac{1 - e^{i2\theta_k 2^l}}{1 - e^{i2\theta_k}} \right|^2 = \left| \frac{1}{2^l} \frac{\sin 2^l \theta_k}{\sin \theta_k} \right|^2 < \left(\frac{1}{2^l} \frac{1}{\frac{\pi}{2^l} |k - k_i - 2^l \delta|} \right)^2 = \frac{1}{4(k - k_i - 2^l \delta)^2}, \quad (B3)$$

where the inequalities $|\sin 2^l \theta_k| \leq 1$ and $|\sin \theta_k| > \frac{2}{\pi} |\theta_k|$ are used. Therefore, we have

$$\sum_{k=0}^{k_{ih}-1} |f_i(k)|^2 < \sum_{k=0}^{k_{ih}-1} \frac{1}{4(k - k_i - 2^l \delta)^2} \leq \sum_{k=0}^{k_{ih}-1} \frac{1}{4(k - k_i)^2} < \int_0^{k_{ih}} \frac{1}{4(k - k_i)^2} dk = \frac{1}{4} \left(\frac{1}{k_i - k_{ih}} - \frac{1}{k_i} \right) < \frac{1}{4 k_i - k_{ih}}. \quad (B4)$$

Similarly, for $1 \leq i \leq M$, $0 \leq E_i t < 2\pi$ and let $\frac{2\pi k_i}{2^l}$ be the best l bit approximation to $E_i t$ which is greater than $E_i t$. The difference between $\frac{2\pi k_i}{2^l}$ and $E_i t$ satisfies $2\pi(\frac{k_i}{2^l} - \delta) = E_i t$ such that $0 \leq \delta < \frac{1}{2^l}$. Let $2\theta_k = \frac{2\pi k}{2^l} - E_i t = \frac{2\pi}{2^l}(k - k_i + 2^l \delta)$, when

$-2^{l-1} \leq k - k_i < 2^{l-1}$ we have $-\frac{\pi}{2} < \theta_k < \frac{\pi}{2}$.

$$|f_i(k)|^2 < \frac{1}{4(k - k_i + 2^l \delta)^2}. \tag{B5}$$

Thus, we have

$$\begin{aligned} \sum_{k_{th}}^{2^l-1} |f_i(k)|^2 &< \sum_{k=k_{th}}^{2^l-1} \frac{1}{4(k - k_i + 2^l \delta)^2} \leq \sum_{k=k_{th}}^{2^l-1} \frac{1}{4(k - k_i)^2} \\ &< \int_{k=k_{th}-1}^{2^l-1} \frac{1}{4(k - k_i)^2} dk = \frac{1}{4} \left(-\frac{1}{2^l - 1 - k_i} + \frac{1}{k_{th} - 1 - k_i} \right) < \frac{1}{4} \frac{1}{k_{th} - 1 - k_i}. \end{aligned} \tag{B6}$$

The upper bound of ϵ_l is

$$\begin{aligned} &\left\| \left(\sum_{i=1}^M \alpha_i \left(\sum_{k=0}^{2^l-1} f_i(k)|k\rangle \right) \otimes |\phi_i\rangle - \sum_{i=M+1}^N \alpha_i \left(\sum_{k=0}^{2^l-1} f_i(k)|k\rangle \right) \otimes |\phi_i\rangle \right) - \sum_{i=1}^N \alpha_i \left(\sum_{k=0}^{k_{th}-1} f_i(k)|k\rangle - \sum_{k_{th}}^{2^l-1} f_i(k)|k\rangle \right) \otimes |\phi_i\rangle \right\| \\ &= \left\| \sum_{i=1}^M \alpha_i \left(2 \sum_{k_{th}}^{2^l-1} f_i(k)|k\rangle \right) \otimes |\phi_i\rangle - \sum_{i=M+1}^N \alpha_i \left(2 \sum_{k=0}^{k_{th}-1} f_i(k)|k\rangle \right) \otimes |\phi_i\rangle \right\| \\ &= \left(4 \sum_{i=1}^M |\alpha_i|^2 \sum_{k_{th}}^{2^l-1} |f_i(k)|^2 + 4 \sum_{i=M+1}^N |\alpha_i|^2 \sum_{k=0}^{k_{th}-1} |f_i(k)|^2 \right)^{\frac{1}{2}} \\ &< \left(4 \sum_{i=1}^M |\alpha_i|^2 \frac{1}{4} \frac{1}{k_{th} - 1 - k_i} + 4 \sum_{i=M+1}^N |\alpha_i|^2 \frac{1}{4} \frac{1}{k_i - k_{th}} \right)^{\frac{1}{2}} \\ &< \left(\sum_{i=1}^M |\alpha_i|^2 \frac{1}{k_{th} - 1 - k_M} + \sum_{i=M+1}^N |\alpha_i|^2 \frac{1}{k_{M+1} - k_{th}} \right)^{\frac{1}{2}} \\ &\leq \left(\sum_{i=1}^M |\alpha_i|^2 \frac{1}{\left\lfloor \frac{2^l(E_M^{(0)} + \Delta/2 - E_M)t}{2\pi} \right\rfloor - 1} + \sum_{i=M+1}^N |\alpha_i|^2 \frac{1}{\left\lfloor \frac{2^l(E_{M+1} - E_M^{(0)} - \Delta/2)t}{2\pi} \right\rfloor - 1} \right)^{\frac{1}{2}} \\ &\leq \max \left\{ \frac{1}{\sqrt{\left\lfloor \frac{2^l(E_M^{(0)} + \Delta/2 - E_M)t}{2\pi} \right\rfloor - 1}}, \frac{1}{\sqrt{\left\lfloor \frac{2^l(E_{M+1} - E_M^{(0)} - \Delta/2)t}{2\pi} \right\rfloor - 1}} \right\}, \end{aligned} \tag{B7}$$

where $k_{th} = \lceil \frac{2^l(E_M^{(0)} + \Delta/2)t}{2\pi} \rceil$, $k_M = \lceil \frac{2^l E_M t}{2\pi} \rceil$, $k_{M+1} = \lfloor \frac{2^l E_{M+1} t}{2\pi} \rfloor$, and $k_M < k_{th} \leq k_{M+1}$. Therefore, we can estimate ϵ_l as

$$O\left(\frac{1}{\sqrt{2^l(E_{M+1} - E_M)t}}\right), \tag{B8}$$

which decreases exponentially with the number of ancilla qubits. The above derivation does not include the special cases $k_M = k_{th}$ ($k_{M+1} = k_{th} - 1$). Note that

$$|f_i(k)|^2 = \frac{1}{2^{2l}} \frac{1 - \cos(\frac{2\pi}{2^l}(k - k_i \pm 2^l \delta)2^l)}{1 - \cos(\frac{2\pi}{2^l}(k - k_i \pm 2^l \delta))} = \frac{1}{2^l} F_{2^l}\left(\frac{2\pi}{2^l}(k - k_i \pm 2^l \delta)\right) \leq 1, \tag{B9}$$

where $F_n(x)$ is the Fejér kernel and $F_n(x) < n$. For the two cases, $|f_M(k_{th})|^2 = |f_{M+1}(k_{th} - 1)|^2 = \frac{1}{2^l} F_{2^l}(2\pi \delta) \leq 1$. Then the error is $O(\frac{1}{\sqrt{2^l(E_{M+1} - E_M)t}}) + |\alpha_M|^2$ or $O(\frac{1}{\sqrt{2^l(E_{M+1} - E_M)t}}) + |\alpha_{M+1}|^2$. If both cases are satisfied, the error is $O(\frac{1}{\sqrt{2^l(E_{M+1} - E_M)t}}) + |\alpha_M|^2 + |\alpha_{M+1}|^2$. We can increase the number of ancilla qubits to avoid such cases.

As a result, the total error (including the failure probability) when realizing $R_{\mathcal{D}}|\Psi\rangle$ is $2^{l+1}\epsilon_l + \epsilon_l$, which is denoted as ϵ_R . Similarly, for $R_{\mathcal{D}_0}$, ϵ_{l0} is $O(\frac{\|H_0\|^2 t^2}{n_T})$, and ϵ_{l0} is $O(\frac{1}{\sqrt{2^l \Delta t}})$. The total error of $R_{\mathcal{D}_0}|\Psi\rangle$ is simplified as ϵ_R , too.

2. The error in realizing U

For U , the controlled unitary gate is $R_{\mathcal{D}_0}R_{\mathcal{D}}$. From Appendix B 1, we see the error of $R_{\mathcal{D}_0}R_{\mathcal{D}}|\Psi\rangle$ is $2\epsilon_R$. Next, we assume $R_{\mathcal{D}_0}R_{\mathcal{D}}$ is perfectly realized. Similarly as in Appendix B 1, we define

$$|a\rangle \equiv \sum_j \beta_j \sum_{k=0}^{2^m-1} g_j(k)|k\rangle \otimes e^{i\frac{\theta_j}{2}}|\psi_j\rangle, \tag{B10}$$

$$|b\rangle \equiv \sum_j \beta_j \sum_{k=0}^{2^m-1} g_j(k)|k\rangle \otimes e^{-i\frac{\pi k}{2^m}}|\psi_j\rangle, \tag{B11}$$

where m is the number of ancilla qubits and $g_j(k) = \frac{1}{2^m} \sum_{x=0}^{2^m-1} e^{i(\frac{2\pi k}{2^m} + \theta_j)x}$.

$-2\pi \leq \theta_j < 0$ and let $-k_j$ be the best m bit approximation to θ_j which is less than θ_j . The difference between $-\frac{2\pi k_j}{2^m}$ and θ_j satisfies $2\pi(-\frac{k_j}{2^m} + \delta) = \theta_j$ such that $0 \leq \delta < \frac{1}{2^m}$. Then

$$|g_j(k)|^2 = \left| \frac{1}{2^m} \frac{1 - e^{i2\pi(\frac{k-k_j}{2^m} + \delta)2^m}}{1 - e^{i2\pi(\frac{k-k_j}{2^m} + \delta)}} \right|^2 = \left(\frac{1}{2^m} \frac{\sin \pi(\frac{k-k_j}{2^m} + \delta)2^m}{\sin \pi(\frac{k-k_j}{2^m} + \delta)} \right)^2 = \frac{1}{2^{2m}} \frac{1 - \cos(2\pi 2^m \delta)}{1 - \cos(\frac{2\pi}{2^m}(k - k_j + 2^m \delta))}, \tag{B12}$$

$$\left| e^{-i\frac{\pi k}{2^m}} - e^{i\frac{\theta_j}{2}} \right|^2 = 2 - 2 \cos\left(-\frac{\pi k}{2^m} - \frac{\theta_j}{2}\right) = 2 - 2 \cos\left(\frac{\pi}{2^m}(k - k_j + 2^m \delta)\right). \tag{B13}$$

Thus the extra error ϵ_m due to the finite ancilla qubits is

$$\begin{aligned} & \left\| \sum_j \beta_j \sum_{k=0}^{2^m-1} g_j(k)|k\rangle \otimes e^{-i\frac{\pi k}{2^m}}|\psi_j\rangle - \sum_j \beta_j \sum_{k=0}^{2^m-1} g_j(k)|k\rangle \otimes e^{i\frac{\theta_j}{2}}|\psi_j\rangle \right\| \\ &= \left(\sum_j |\beta_j|^2 \sum_{k=0}^{2^m-1} |g_j(k)|^2 \left| e^{-i\frac{\pi k}{2^m}} - e^{i\frac{\theta_j}{2}} \right|^2 \right)^{\frac{1}{2}} \\ &= \left(\sum_j |\beta_j|^2 \sum_{k=0}^{2^m-1} \frac{1 - \cos(2\pi 2^m \delta)}{2^{2m}} \frac{1 - \cos(\frac{\pi}{2^m}(k - k_j + 2^m \delta))}{1 - \cos(\frac{2\pi}{2^m}(k - k_j + 2^m \delta))} \right)^{\frac{1}{2}} \\ &\leq \left(\sum_j |\beta_j|^2 \sum_{k=0}^{2^m-1} \frac{4}{2^{2m}} \frac{1 - \cos(\frac{\pi}{2^m}(k - k_j + 2^m \delta))}{2 \sin^2(\frac{\pi}{2^m}(k - k_j + 2^m \delta))} \right)^{\frac{1}{2}} \\ &< \left(\sum_j |\beta_j|^2 \sum_{k=0}^{2^m-1} \frac{4}{2^{2m}} \frac{\frac{1}{2} \frac{\pi^2}{2^{2m}}(k - k_j + 2^m \delta)^2}{2 \frac{4}{\pi^2} \frac{\pi^2}{2^{2m}}(k - k_j + 2^m \delta)^2} \right)^{\frac{1}{2}} \\ &= \left(\sum_j |\beta_j|^2 \sum_{k=0}^{2^m-1} \frac{1}{2^{2m}} \frac{\pi^2}{4} \right)^{\frac{1}{2}} \\ &= \left(\frac{1}{2^m} \frac{\pi^2}{4} \right)^{\frac{1}{2}} \\ &= \frac{\pi}{2^{m/2+1}}. \end{aligned} \tag{B14}$$

Therefore, the total error of the algorithm is given by

$$\begin{aligned} \epsilon_{tot} &\sim 2^{m+2}\epsilon_R + \epsilon_m \\ &\sim 2^{m+2}(2^{l+1}\epsilon_t + \epsilon_l) + \epsilon_m, \end{aligned} \tag{B15}$$

where ϵ_t is $O(\frac{\|H\|^2 t^2}{n_T})$, ϵ_l is $O(\frac{1}{\sqrt{2^{l(E_{M+1}-E_M)}t}})$, and ϵ_m is $O(\frac{1}{\sqrt{2^m}})$.

APPENDIX C: DETAILED STEPS OF THE TAYLOR EXPANSION OF \mathcal{L}_t

The Taylor series of e^{-iHt} is

$$I - iHt - \frac{1}{2}H^2t^2 + O(t^3). \tag{C1}$$

Substituting this into Eq. (22) yields

$$\begin{aligned} \mathcal{L}_t &= -\frac{1}{M} \sum_{i,j} \left| \langle \phi_i^{(0)} | U(I - iHt - \frac{1}{2}H^2t^2 + O(t^3))U^\dagger | \phi_j^{(0)} \rangle \right|^2 \\ &= -\frac{1}{M} \sum_{i=j} \left| 1 - it \langle \phi_i^{(0)} | UHU^\dagger | \phi_i^{(0)} \rangle - \frac{1}{2}t^2 \langle \phi_i^{(0)} | UH^2U^\dagger | \phi_i^{(0)} \rangle + O(t^3) \right|^2 \\ &\quad - \frac{1}{M} \sum_{i \neq j} \left| -it \langle \phi_i^{(0)} | UHU^\dagger | \phi_j^{(0)} \rangle - \frac{1}{2}t^2 \langle \phi_i^{(0)} | UH^2U^\dagger | \phi_j^{(0)} \rangle + O(t^3) \right|^2 \\ &= -\frac{1}{M} \sum_{i=j} \left[\left(1 - \frac{1}{2}t^2 \langle \phi_i^{(0)} | UH^2U^\dagger | \phi_i^{(0)} \rangle \right)^2 + t^2 \langle \phi_i^{(0)} | UHU^\dagger | \phi_i^{(0)} \rangle^2 \right] \\ &\quad - \frac{1}{M} \sum_{i \neq j} \left| -it \langle \phi_i^{(0)} | UHU^\dagger | \phi_j^{(0)} \rangle \right|^2 + O(t^3) \\ &= -\frac{1}{M} \sum_{i=j} \left(1 - t^2 \langle \phi_i^{(0)} | UH^2U^\dagger | \phi_i^{(0)} \rangle + t^2 \langle \phi_i^{(0)} | UHU^\dagger | \phi_i^{(0)} \rangle^2 \right) \\ &\quad - \frac{1}{M} \sum_{i \neq j} t^2 \left| \langle \phi_i^{(0)} | UHU^\dagger | \phi_j^{(0)} \rangle \right|^2 + O(t^3) \\ &= -1 + \frac{t^2}{M} \left(\sum_{i=1}^M \langle \phi_i^{(0)} | UH^2U^\dagger | \phi_i^{(0)} \rangle - \sum_{i,j} \left| \langle \phi_i^{(0)} | UHU^\dagger | \phi_j^{(0)} \rangle \right|^2 \right) + O(t^3). \tag{C2} \end{aligned}$$

APPENDIX D: EQUIVALENCE OF THE COMPLETE BLOCK DIAGONALIZATION OF H

Recall that P is the projector in low-energy subspace \mathcal{P} of H , Q is its orthogonal complement which represents the high-energy subspace projector. They can be written as

$$P = \sum_{i=1}^M U^\dagger | \phi_i^{(0)} \rangle \langle \phi_i^{(0)} | U = \sum_{i=1}^M | \phi_i \rangle \langle \phi_i |, \tag{D1}$$

$$Q = \sum_{i=M+1}^N U^\dagger | \phi_i^{(0)} \rangle \langle \phi_i^{(0)} | U = \sum_{i=M+1}^N | \phi_i \rangle \langle \phi_i |. \tag{D2}$$

With Eq. (D1), C can be converted to

$$\begin{aligned} C &= \sum_{i=1}^M \langle \phi_i | H^2 | \phi_i \rangle - \sum_{i,j} \left| \langle \phi_i | H | \phi_j \rangle \right|^2 \\ &= \sum_{i=1}^M \langle \phi_i | H^2 | \phi_i \rangle - \sum_{i,j} \langle \phi_i | H | \phi_j \rangle \langle \phi_j | H | \phi_i \rangle \\ &= \text{Tr}(PH^2P) - \text{Tr}(PHPHP), \tag{D3} \end{aligned}$$

where the trace operation acts on the Hilbert space of whole system.

Define

$$H_P = PHP, \tag{D4}$$

$$H_Q = QHQ, \tag{D5}$$

$$H_{PQ} = PHQ, \tag{D6}$$

$$H_{QP} = QHP. \tag{D7}$$

The Hamiltonian can be divided into

$$H = H_P + H_Q + H_{PQ} + H_{QP}, \tag{D8}$$

and its square is

$$\begin{aligned} H^2 &= H_P^2 + H_P H_{PQ} + H_Q^2 + H_Q H_{QP} + H_{PQ} H_Q \\ &\quad + H_{PQ} H_{QP} + H_{QP} H_P + H_{QP} H_{PQ}. \tag{D9} \end{aligned}$$

So, we have

$$PH^2P = H_P^2 + H_{PQ} H_{QP}. \tag{D10}$$

Substituting Eq. (D4) and Eq. (D10) into Eq. (D3), we get

$$\begin{aligned} C &= \text{Tr}(PH^2P) - \text{Tr}(PHPHP) \\ &= \text{Tr}(H_P^2) + \text{Tr}(H_{PQ} H_{QP}) - \text{Tr}(H_P^2) \\ &= \text{Tr}(H_{PQ} H_{QP}). \tag{D11} \end{aligned}$$

Therefore, $C = 0$ if and only if H_{PQ} is a zero matrix which indicates H is completely block-diagonal with respect to P and Q .

APPENDIX E: GENERAL CASE OF SWT

In a general situation, the unperturbed Hamiltonian is

$$H_0 = \sum_{i=1}^K E_i^{(0)} |\phi_i^{(0)}\rangle\langle\phi_i^{(0)}| + \sum_{i=K+1}^{K+M} E_i^{(0)} |\phi_i^{(0)}\rangle\langle\phi_i^{(0)}| + \sum_{i=K+M+1}^N E_i^{(0)} |\phi_i^{(0)}\rangle\langle\phi_i^{(0)}|, \tag{E1}$$

with eigenvalues $E_1^{(0)} \leq \dots \leq E_K^{(0)} < E_{K+1}^{(0)} \leq \dots \leq E_{K+M}^{(0)} < E_{K+M+1}^{(0)} \leq \dots \leq E_N^{(0)}$. The projector onto the eigenspace of eigenvalues $E_i^{(0)} \in [E_{K+1}^{(0)}, E_{K+M}^{(0)}]$ reads

$$P_0 = \sum_{i=K+1}^{K+M} |\phi_i^{(0)}\rangle\langle\phi_i^{(0)}|. \tag{E2}$$

Here the energy gap is

$$\Delta = \min\{E_{K+1}^{(0)} - E_K^{(0)}, E_{K+M+1}^{(0)} - E_{K+M}^{(0)}\}. \tag{E3}$$

Through the same assumption Eq. (4), the total Hamiltonian can be written as

$$H = \sum_{i=1}^K E_i |\phi_i\rangle\langle\phi_i| + \sum_{i=K+1}^{K+M} E_i |\phi_i\rangle\langle\phi_i| + \sum_{i=K+M+1}^N E_i |\phi_i\rangle\langle\phi_i|, \tag{E4}$$

with eigenvalues $E_1 \leq \dots \leq E_K < E_{K+1} \leq \dots \leq E_{K+M} < E_{K+M+1} \leq \dots \leq E_N$. The eigenspace \mathcal{P} is spanned by H 's eigenstates with eigenvalues $E_i \in (E_{K+1} - \Delta/2, E_{K+M} + \Delta/2)$. Then the effective energy spectra, from E_{K+1} to E_{K+M} , can be obtained following the same method.

[1] G. Vidal, Efficient Simulation of One-Dimensional Quantum Many-Body Systems, *Phys. Rev. Lett.* **93**, 040502 (2004).

[2] R. Islam, R. Ma, P. M. Preiss, M. E. Tai, A. Lukin, M. Rispoli, and M. Greiner, Measuring entanglement entropy in a quantum many-body system, *Nature* **528**, 77 (2015).

[3] G. Carleo and M. Troyer, Solving the quantum many-body problem with artificial neural networks, *Science* **355**, 602 (2017).

[4] C. E. Soliverz, General theory of effective Hamiltonians, *Phys. Rev. A* **24**, 4 (1981).

[5] J. R. Schrieffer and P. A. Wolff, Relation between the Anderson and Kondo Hamiltonians, *Phys. Rev.* **149**, 491 (1966).

[6] S. Bravyi, D. P. DiVincenzo, and D. Loss, Schrieffer-Wolff transformation for quantum many-body systems, *Ann. Phys.* **326**, 2793 (2011).

[7] A. H. MacDonald, S. M. Girvin, and D. Yoshioka, $\frac{1}{V}$ expansion for the Hubbard model, *Phys. Rev. B* **37**, 9753 (1988).

[8] P. Fazekas, *Lecture Notes on Electron Correlation and Magnetism* (World Scientific, Singapore, 1999), Vol. 5.

[9] C. L. Cleveland and R. Medina A, Obtaining a Heisenberg Hamiltonian from the Hubbard model, *Am. J. Phys.* **44**, 44 (1976).

[10] J. Paaske and K. Flensberg, Vibrational Sidebands and the Kondo Effect in Molecular Transistors, *Phys. Rev. Lett.* **94**, 176801 (2005).

[11] M. Issler, E. M. Kessler, G. Giedke, S. Yelin, I. Cirac, M. D. Lukin, and A. Imamoglu, Nuclear Spin Cooling Using Overhauser-Field Selective Coherent Population Trapping, *Phys. Rev. Lett.* **105**, 267202 (2010).

[12] U. Hohenester, Cavity quantum electrodynamics with semiconductor quantum dots: Role of phonon-assisted cavity feeding, *Phys. Rev. B* **81**, 155303 (2010).

[13] S. I. Erlingsson, J. C. Egues, and D. Loss, Energy spectra for quantum wires and two-dimensional electron gases in magnetic fields with Rashba and Dresselhaus spin-orbit interactions, *Phys. Rev. B* **82**, 155456 (2010).

[14] B. Uchoa, T. G. Rappoport, and A. H. Castro Neto, Kondo Quantum Criticality of Magnetic Adatoms in Graphene, *Phys. Rev. Lett.* **106**, 016801 (2011).

[15] E. M. Kessler, Generalized Schrieffer-Wolff formalism for dissipative systems, *Phys. Rev. A* **86**, 012126 (2012).

[16] T. T. Heikkilä, F. Massel, J. Tuorila, R. Khan, and M. A. Sillanpää, Enhancing Optomechanical Coupling via the Josephson Effect, *Phys. Rev. Lett.* **112**, 203603 (2014).

[17] M. Bukov, L. D'Alessio, and A. Polkovnikov, Universal high-frequency behavior of periodically driven systems: from dynamical stabilization to Floquet engineering, *Adv. Phys.* **64**, 139 (2015).

[18] M. Bukov, M. Kolodrubetz, and A. Polkovnikov, Schrieffer-Wolff Transformation for Periodically Driven Systems: Strongly Correlated Systems with Artificial Gauge Fields, *Phys. Rev. Lett.* **116**, 125301 (2016).

[19] G. Zhang, E. Novais, and H. U. Baranger, Rescuing a Quantum Phase Transition with Quantum Noise, *Phys. Rev. Lett.* **118**, 050402 (2017).

[20] K. H. Matlack, M. Serra-Garcia, A. Palermo, S. D. Huber, and C. Daraio, Designing perturbative metamaterials from discrete models, *Nat. Mater.* **17**, 323 (2018).

[21] F. Yan, P. Krantz, Y. Sung, M. Kjaergaard, D. L. Campbell, T. P. Orlando, S. Gustavsson, and W. D. Oliver, Tunable Coupling Scheme for Implementing High-Fidelity Two-Qubit Gates, *Phys. Rev. Appl.* **10**, 054062 (2018).

[22] J. Wurtz, P. W. Claeys, and A. Polkovnikov, Variational Schrieffer-Wolff transformations for quantum many-body dynamics, *Phys. Rev. B* **101**, 014302 (2020).

[23] L. Garbe, M. Bina, A. Keller, M. G. A. Paris, and S. Felicetti, Critical Quantum Metrology with a Finite-Component Quantum Phase Transition, *Phys. Rev. Lett.* **124**, 120504 (2020).

[24] Y. Murakami, S. Takayoshi, A. Koga, and P. Werner, High-harmonic generation in one-dimensional Mott insulators, *Phys. Rev. B* **103**, 035110 (2021).

- [25] L. L. Foldy and S. A. Wouthuysen, On the dirac theory of spin 1/2 particles and its non-relativistic limit, *Phys. Rev.* **78**, 29 (1950).
- [26] H. Fröhlich, Interaction of electrons with lattice vibrations, *Proc. R. Soc. London A* **215**, 291 (1952).
- [27] R. Winkler, S. Papadakis, E. De Poortere, and M. Shayegan, *Spin-Orbit Coupling in Two-Dimensional Electron and Hole Systems* (Springer, New York, 2003), Vol. 41
- [28] M. Wagner, *Unitary Transformations in Solid State Physics* (North-Holland, Amsterdam, 1986).
- [29] P. W. Shor, Algorithms for quantum computation: Discrete logarithms and factoring, in *Proceedings of the 35th Annual Symposium on Foundations of Computer Science* (IEEE, Santa Fe, 1994), pp. 124–134.
- [30] F. Arute, K. Arya, R. Babbush, D. Bacon, J. C. Bardin, R. Barends, R. Biswas, S. Boixo, F. G. Brandao, D. A. Buell *et al.*, Quantum supremacy using a programmable superconducting processor, *Nature* **574**, 505 (2019).
- [31] P. W. Shor, Fault-tolerant quantum computation, in *Proceedings of the 37th Conference on Foundations of Computer Science* (IEEE, Burlington, 1996), pp. 56–65.
- [32] D. Gottesman, Theory of fault-tolerant quantum computation, *Phys. Rev. A* **57**, 127 (1998).
- [33] J. Preskill, Quantum computing in the NISQ era and beyond, *Quantum* **2**, 79 (2018).
- [34] A. Peruzzo, J. McClean, P. Shadbolt, M.-H. Yung, X.-Q. Zhou, P. J. Love, A. Aspuru-Guzik, and J. L. O’Brien, A variational eigenvalue solver on a photonic quantum processor, *Nat. Commun.* **5**, 4213 (2014).
- [35] M. Cerezo, A. Arrasmith, R. Babbush, S. C. Benjamin, S. Endo, K. Fujii, J. R. McClean, K. Mitarai, X. Yuan, L. Cincio *et al.*, Variational quantum algorithms, *Nat. Rev. Phys.* **3**, 625 (2021).
- [36] A. Kandala, A. Mezzacapo, K. Temme, M. Takita, M. Brink, J. M. Chow, and J. M. Gambetta, Hardware-efficient variational quantum eigensolver for small molecules and quantum magnets, *Nature* **549**, 242 (2017).
- [37] Y. Li and S. C. Benjamin, Efficient Variational Quantum Simulator Incorporating Active Error Minimization, *Phys. Rev. X* **7**, 021050 (2017).
- [38] E. Farhi and H. Neven, Classification with quantum neural networks on near term processors, [arXiv:1802.06002](https://arxiv.org/abs/1802.06002).
- [39] X. Xu, J. Sun, S. Endo, Y. Li, S. C. Benjamin, and X. Yuan, Variational algorithms for linear algebra, *Sci. Bull.* **66**, 2181 (2021).
- [40] T. Jones and S. Benjamin, Questlink-mathematica embiggened by a hardware-optimised quantum emulator, *Quantum Sci. Technol.* **5**, 034012 (2020).
- [41] R. U. Haq and K. Singh, A systematic method for Schrieffer-Wolff transformation and its generalizations, [arXiv:2004.06534](https://arxiv.org/abs/2004.06534).
- [42] G. Consani and P. A. Warburton, Effective Hamiltonians for interacting superconducting qubits: Local basis reduction and the Schrieffer-Wolff transformation, *New J. Phys.* **22**, 053040 (2020).
- [43] F. Arute, K. Arya, R. Babbush, D. Bacon, J. C. Bardin, R. Barends, A. Bengtsson, S. Boixo, M. Broughton, B. B. Buckley *et al.*, Observation of separated dynamics of charge and spin in the Fermi-Hubbard model, [arXiv:2010.07965](https://arxiv.org/abs/2010.07965).
- [44] F. C. Zhang and T. M. Rice, Effective Hamiltonian for the superconducting cu oxides, *Phys. Rev. B* **37**, 3759 (1988).
- [45] C. D. Batista and A. A. Aligia, Effective Hamiltonian for cuprate superconductors, *Phys. Rev. B* **47**, 8929 (1993).
- [46] M. Hirayama, T. Miyake, M. Imada, and S. Biermann, Low-energy effective Hamiltonians for correlated electron systems beyond density functional theory, *Phys. Rev. B* **96**, 075102 (2017).
- [47] A. Blais, A. L. Grimsmo, S. M. Girvin, and A. Wallraff, Circuit quantum electrodynamics, *Rev. Mod. Phys.* **93**, 025005 (2021).
- [48] P. Gartner and V. Moldoveanu, Effective Hamiltonians in the quantum Rabi problem, *Phys. Rev. A* **105**, 023704 (2022).
- [49] B. Delamotte, An introduction to the nonperturbative renormalization group, in *Renormalization Group and Effective Field Theory Approaches to Many-Body Systems* (Springer, New York, 2012), pp. 49–132.
- [50] K. Tsukiyama, S. K. Bogner, and A. Schwenk, In-Medium Similarity Renormalization Group for Nuclei, *Phys. Rev. Lett.* **106**, 222502 (2011).
- [51] S. R. White, Numerical canonical transformation approach to quantum many-body problems, *J. Chem. Phys.* **117**, 7472 (2002).
- [52] S. Nakayama, A. Soeda, and M. Murao, Quantum Algorithm for Universal Implementation of the Projective Measurement of Energy, *Phys. Rev. Lett.* **114**, 190501 (2015).
- [53] A. K. Ekert, C. M. Alves, D. K. L. Oi, M. Horodecki, P. Horodecki, and L. C. Kwok, Direct Estimations of Linear and Nonlinear Functionals of a Quantum State, *Phys. Rev. Lett.* **88**, 217901 (2002).
- [54] K. Mitarai and K. Fujii, Methodology for replacing indirect measurements with direct measurements, *Phys. Rev. Res.* **1**, 013006 (2019).
- [55] Y. Li, T. Shi, B. Chen, Z. Song, and C.-P. Sun, Quantum-state transmission via a spin ladder as a robust data bus, *Phys. Rev. A* **71**, 022301 (2005).
- [56] J. C. Spall, Implementation of the simultaneous perturbation algorithm for stochastic optimization, *IEEE Trans. Aerosp. Electron. Syst.* **34**, 817 (1998).
- [57] P. Czarnik, A. Arrasmith, P. J. Coles, and L. Cincio, Error mitigation with Clifford quantum-circuit data, *Quantum* **5**, 592 (2021).
- [58] A. Strikis, D. Qin, Y. Chen, S. C. Benjamin, and Y. Li, Learning-based quantum error mitigation, *PRX Quantum* **2**, 040330 (2021).
- [59] IBM Quantum, <https://quantum-computing.ibm.com/> (2021).
- [60] S. Lloyd, Universal quantum simulators, *Science* **273**, 1073 (1996).